Eur Biophys J (1994) 23:307–322

European Biophysics Journal

Hydrodynamics of segmentally flexible macromolecules

J. Garcia de la Torre

Departamento de Quimica Fisica, Universidad de Murcia, E-30071 Murcia, Spain

Received: 28 June 1994 / Accepted: 12 July 1994

Abstract. Segmentally flexible macromolecules are composed of a few rigid subunits linked by joints which are more or less flexible. The dynamics in solution of this type of macromolecule present special aspects that are reviewed here. Three alternative approaches are described. One is the rigid-body treatment, which is shown to be valid for overall dynamic properties such as translational diffusion and intrinsic viscosity. Another approach is the Harvey-Wegener treatment, which is particularly suited for rotational diffusion. The simplest version of this treatment, which ignores hydrodynamic interaction (HI) effects, is found to be quite accurate when compared to a more rigorous version including HI. A third approach is the Brownian dynamics simulation that, albeit at some computational cost, might describe rigorously cases of arbitrary complexity. This technique has been used to test the approximations in the rigid-body and Harvey-Wegener treatments, thus allowing a better understanding of their validity. Brownian trajectories of simplified models such as the trumbbell and the broken rod have been simulated. The comparison of the decay rates of some correlation functions with the predictions of the two treatments leads to a general conclusion: the Harvey-Wegener treatment determines the initial rate, while the long-time behavior is dominated by the rigid-body relaxation time. As an example of application to a specific biological macromolecule, we present a simulation of an immunoglobulin molecule, showing how Brownian Dynamics can be used to predict rotational and internal dynamics. Another typical example is myosin. Literature data of hydrodynamic properties of whole myosin and the myosin rod are compared with predictions from the Harvey-Wegener and rigid-body treatments. The present situation of the problem on myosin flexibility is analyzed, and some indications are given for future experimental and simulation work.

Key words: Hydrodynamics – Segmental flexibility – Diffusion coefficients – Myosin – Antibodies

1. Introduction

1.1. Semiflexible macromolecules

Generally speaking, biological macromolecules can be classified into two general types, rigid and flexible. The chain of covalent bonds that forms the macromolecular entity is in principle flexible and therefore able to present a variety of conformations. However, in many cases of biological interest, there are a number of intramolecular interactions within the chain (van der Waals, hydrogen bonds, covalent bridges) that make one of the conformations much more probable than all the others, and determines a specific shape for the macromolecule. Without the conformational variability, the macromolecule can be regarded as a rigid particle. On the other hand, if there are no such interactions, the flexibility of the chain will make it behave as a random coil (this is indeed the case for most synthetic polymers). The flexibility of biological macromolecules plays an essential role in their physiological function. In the rigid case, that role is determined by the peculiarities of the shape, while in the flexible ones, the function is usually linked to flexibility.

The above classification is not clear-cut but instead represents two extreme limits. There are a number of biological macromolecules with an intermediate behavior between the two limits, that is not well described by either of them. They are what we call semiflexible macromolecules. Within them we can distinguish (as limiting situations, again), two different types. In one of them, flexibility takes place evenly throughout the entire macromolecule. A well known example is double helical DNA (Bloomfield et al. 1974). The DNA helix is locally rigid and a DNA fragment, if it is short enough, looks like a rigid, straight rod. However, if the length of the DNA exceeds a characteristic length, the conformation is somehow variable, and the DNA looks like a bending rod, or wormlike coil. In this case, the flexibility is distributed all along the contour length of the helix.

In another type of semiflexible macromolecule, the structure is essentially rigid everywhere except in a few,

localized regions that are more or less flexible. In contrast to the former type, flexibility is now localized in a few sites in the macromolecule, which behaves as a set of rigid parts (also called subunits, or segments) linked by partially flexible hinges (also called joints or swivels). It is said that macromolecules of this type are hinged (Harvey 1978, 1979), swivel-jointed (Wegener 1980, 1982a, b) or segmentally flexible (Yguerabide et al. 1970).

The conformation and dynamics of wormlike macromolecules have been the subject of many studies for almost fifty years, and the main results can be found in monographs and textbooks (Yamakawa 1971; Bloomfield 1974; Cantor and Schimmel 1980; Richards 1980). The theoretical approach to segmentally flexible macromolecules is more recent and has gone through a different route. In the present article we will cover this second type, although some mention of wormlike macromolecules will be made when necessary.

1.2. Solution properties

The properties in dilute solution are traditionally the main sources of information about the overall structure, including shape and flexibility, of a biological macromolecule (The structure at nearly atomic level is probed, for instance, by crystallography, but this structural level is outside the scope of this article). These properties have the advantage over other visualization methods, such as microscopy, that they do not require artificial handling which could introduce distortions; instead, the measurements can be made in conditions rather close to the physiological ones. Some of them are equilibrium properties, the radius of gyration being a typical example, while many others are of dynamic nature. There are some hydrodynamic properties whose definition or significance is similar for rigid and flexible macromolecules. Such is the case for the translational diffusion coefficient and the sedimentation coefficients, which correspond to the overall translational displacement of the particle. In some respects, the situation is similar for the intrinsic viscosity.

There are other, more involved hydrodynamic techniques, that rather than yielding a numerical value for a single coefficient, instead provide a time-dependent correlation or decay function, with more information content. Examples are phosphorescence and fluorescence anisotropy decay (Bayley and Dale 1985), transient electric birefringence or dichroism (Frederick and Houssier 1973; Jennings 1985), dynamic light scattering (Berne and Pecora 1976; Bloomfield 1985a, b; Harding and Rowe 1992) and NMR relaxation (Abragam 1978). These techniques monitor the reorientation, due to rotational or internal Brownian motion, of the whole macromolecule or its parts, depending on the case. For a rigid macromolecule they are governed by rigid-body rotational diffusion, which in turn is determined by a reduced set of diffusion coefficients or relaxation times (Wegener et al. 1979). However, for a flexible entity, we cannot speak of an overall rotation because the particle does not rotate as a whole; instead, the motion of every part or segment is somehow coupled to that of the other parts, in a way and to an extent that must depend strongly on the type and degree of flexibility. Then, those electro-optical and spectroscopic techniques are rich sources of information about semiflexible macromolecules. In the present paper we will pay attention to the prediction or interpretation of their results in the particular cases of segmentally flexible macromolecules.

1.3. Examples of segmentally flexible macromolecules and models

There are a variety of macromolecules that can be ascribed to this type. A simple, clear example is that of some polypeptides that are synthesized from a bifunctional initiator with some internal flexibility. In helicogenic solvents, they adopt a rigid helical (rodlike) conformation, except precisely at the site where the initiator is. The macromolecule behaves as a broken rod, having two rodlike segments joined by a hinge (Matsumoto et al. 1975; Muroaga et al. 1988; Ulyanova 1992).

Myosin has often been cited as a typical semiflexible macromolecule. This protein has two almost globular heads, the S1 fragments, joined to a long, thin rod. The myosin rod has two regions called S2 and LMM subfragments. Although the rod may have some wormlike character, it has been assumed in some work that the S2 and LMM are straight rods joined by a semiflexible hinge. The two partially flexible joints in the myosin molecule are important in the Huxley (1971) mechanism of muscle contraction, and therefore much effort has been devoted to the solution properties of the molecule, looking for information on its flexibility (Harvey and Cheung 1982; Lopez Lacomba et al. 1989). Other biological macromolecules that have usually been regarded as segmentally flexible macromolecules are antibodies (Burton 1987). They have three supposedly rigid segments (two Fab's and one Fc) linked at a single joint. Indeed the "segmentally flexible" terms was coined by Stryer and coworkers (Yguerabide et al. 1970; see also Oi et al. 1984), in their studies on the characterization of the flexibility of antibodies, which seems to be related closely to their function in physiological processes (Gregory et al. 1987). There are a number of other proteins that are assumed to be hinged; calmodulin is an interesting, recently characterized case (Barbato et al. 1992).

For the calculation of hydrodynamic properties, macromolecules are represented by physical models. Some models for segmentally flexible macromolecules are displayed in Fig. 1. An obvious example is the broken rod (Fig. 1 A), in which the flexing at the hinge may be either free or restricted. If two globular elements are joined flexibly at one of the ends of the broken rod, we have a model for whole myosin (Fig. 1 B). For the convenience of hydrodynamic treatment of these particles, the rigid parts are modelled as arrays of spherical elements, or beads, as indicated in Fig. 1 C for the broken rod. One of those beads can represent a joint. The so-called "trumbbell" (Hassager 1974; Roitman and Zimm 1984a, b) is a very simple segmentally flexible model with two links joining three beads, of which the central one

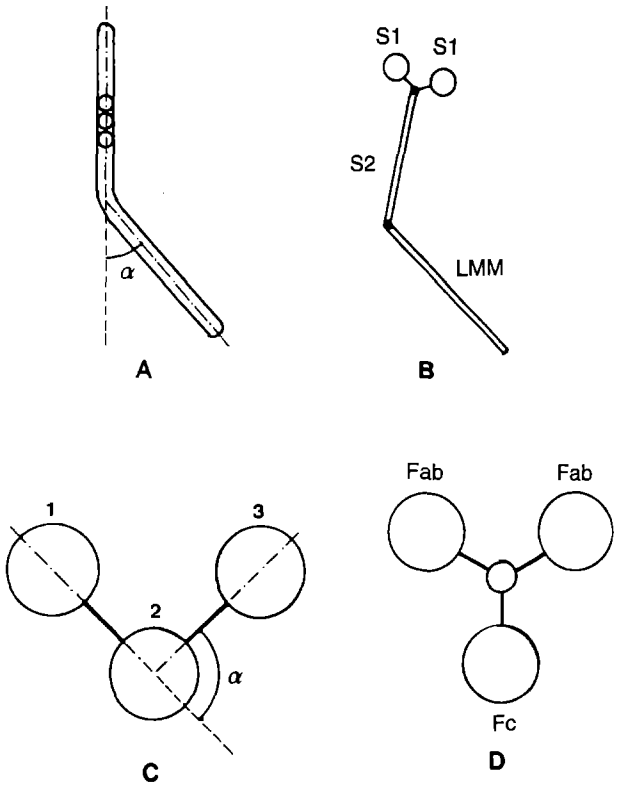

Fig. 1. **A** Broken rod, modeled as a string of beads, showing the definition of the angle, α between the two arms. **B** Simple model for a myosin molecule (see also Fig. 2a). **C** The trumbbell model. **D** Model for a immunoglobulin molecule.

acts as the hinge (Fig. 1 C). As in the broken rod (of which the trumbbell is the simplest case) the hinge-bending motion may be somehow restricted. Another interesting and simple model, which has been employed for antibodies (Diaz et al. 1990), with three elements and a hinge is presented in Fig. 1 D.

2. Rigid-body treatment

The understanding of the hydrodynamics of rigid bodies is essential for the description of the hydrodynamics of segmentally flexible particles in two senses. First, there is an approximate theoretical approach for flexible particles, the so-called rigid body treatment, that allows the calculation of some properties using rigid-body theory. From another point of view, a rigorous theory of the dynamics of segmentally flexible particles can be developed by generalization of the theory of rigid particles. That theory is now well established, and it has been reviewed elsewhere (Garcia de la Torre 1981; Garcia de la Torre and Bloomfield 1981; Garcia de la Torre 1989). Here only the aspects that are relevant for the subsequent description of segmentally flexible macromolecule will be summarized.

A general rigid particle has six degrees of freedom, three for translation and three for rotations. Accordingly, both the frictional resistance to motion and the diffusivity are characterized by means of symmetric matrices of dimension 6×6, which are respectively the friction tensor, $\mathscr{D}$ and the diffusion tensor Ξ. A generalized Einstein relationship holds between $\mathscr{D}$ and Ξ

$$\mathscr{D} = kT\Xi^{-1} \tag{1}$$

where k is Boltzmann constant and T the absolute temperature. It is convenient to divide $\mathscr{D}$ and Ξ into four 3×3 blocks which correspond to translation (tt), rotation (rr) and translation-rotation coupling (tr). Thus, Eq. (1) can be rewritten as

$$\begin{pmatrix} \mathbf{D}_{tt} & \mathbf{D}_{tr}^{T} \\ \mathbf{D}_{tr} & \mathbf{D}_{rr} \end{pmatrix} = kT \begin{pmatrix} \Xi_{tt} & \Xi_{tr}^{T} \\ \Xi_{tr} & \Xi_{rr} \end{pmatrix}^{-1}. \tag{2}$$

In Eq. (2), the superscript T denotes transposition.

Some important hydrodynamic properties can be obtained from the components of the diffusion tensor. Thus, the translational diffusion coefficient D_t is given by the mean of the diagonal components of $\mathbf{D}_{tt}$

$$D_t = \tfrac{1}{3}\mathrm{Tr}\,\mathbf{D}_{tt}. \tag{3}$$

The sedimentation coefficient can be obtained directly from D_t by means of the Svedberg equation (Cantor and Schimmel 1980; Richards 1980). Similarly, the rotational dynamics are entirely determined by the $\mathbf{D}_{rr}$ block. For a rigid body of arbitrary size, all the manifestations of rotational Brownian motion can be described by a set of five relaxation times, the longest of which is (Wegener et al. 1979):

$$\tau_1 = (6D - 2\Delta)^{-1} \tag{4}$$

where D and Δ are respectively the mean and the anisotropy of the eigenvalues of the $\mathbf{D}_{rr}$ bock. All the other relaxation times again depend exclusively on the three eigenvalues. Thus the evaluation of diffusion coefficients and relaxation times is made from the blocks of $\mathscr{D}$, which in turn must be calculated from the blocks of Ξ using Eq. (2). The calculation of the blocks of Ξ can be made from basic hydrodynamic theory in the simplest cases of spherical or ellipsoidal particles. For particles of arbitrary shape, the calculation can be made using bead models (Bloomfield et al. 1967; Garcia de la Torre and Bloomfield 1977), in which the detailed shape of the particle is modeled using spherical beads, either identical or unequal. The equations for the bead-model calculation of the components of the friction tensor are described elsewhere (Garcia de la Torre 1981; Garcia de la Torre and Bloomfield 1981; Garcia de la Torre 1989). In addition to these coefficients, the evaluation of zero-shear intrinsic viscosity and viscoelastic properties requires some additional formalism beyond the Stokes-Einstein equation, but the methodology and the bead-model calculation are very similar (Garcia de la Torre and Bloomfield 1978; Garcia de la Torre 1981, 1989; Wegener 1985).

In contrast to rigid particles, flexible macromolecules do not show a unique shape but, instead, as a consequence of flexibility, the present a variety of conformations. The equilibrium properties of flexible macromolecules are averages over the values calculated for each possible conformation. Formally, if we describe individual conformations by means of a set of internal coordinates

$q_1, q_2, \ldots$, then both the considered property $P(q_1, q_2, \ldots)$ and the potential energy, $V(q_1, q_2, \ldots)$ would be functions of the internal coordinates. Then, the observed value of the property would be the average

$$\langle P \rangle = \frac{\int \cdots \int P(q_1, q_2, \ldots)\, e^{-V(q_1, q_2, \ldots)/kT}\, d\tau}{\int \cdots \int e^{-V(q_1, q_2, \ldots)/kT}\, d\tau}$$

where the multiple integral corresponds to the set of internal coordinates, and $d\tau$ is the differential of volume, i.e., the product of the dq's with the appropriate metric factor. As a particular example, let us consider the simple case of a segmentally flexible macromolecule with two elongated subunits having revolution symmetry. A typical example is a broken rod, as in Fig. 1 a. A single internal coordinate suffices, namely the angle α between the subunit axes. Then the observable properties are given by

$$\langle P \rangle = \frac{\int_0^\pi P(\alpha)\, e^{-V(\alpha)/kT} \sin(\alpha)\, d\alpha}{\int_0^\pi e^{-V(\alpha)/kT} \sin(\alpha)\, d\alpha}. \tag{5}$$

Usually the $\langle \ldots \rangle$ brackets are not written, because it is obvious that some properties of flexible macromolecules are averages.

This is in summary the rigid-body treatment for flexible macromolecules. This treatment is indeed absolutely rigorous for equilibrium properties such as macromolecular dimensions (radius of gyration), total-intensity light or x-ray scattering, steady-state electric birefringence or dichroism, and many others. For hydrodynamic properties, the rigid-body treatment is just an approximation that can be very useful if it is used carefully. The translational diffusion coefficient and the intrinsic viscosity are properties that reflect the overall dynamics of the macromolecule and can be calculated this way within a few percent of the exact values (Wegener 1985). For properties that depend on rotational diffusion, however, much caution has to be used in the application of the rigid-body treatment. Within this treatment, a longest relaxation time can be defined as the conformational average of Eq. (4):

$$1/\tau_{rb} = \langle 6D - 2\Delta \rangle. \tag{6}$$

For very stiff macromolecules, which present minor conformational fluctuations over a most stable conformation, τ_{rb} will dominate most of the decay of electric birefringence or dichroism (Hagerman and Zimm 1987) or that of correlation functions in dynamic light scattering. If the particle is moderately flexible, this may not be valid. A rigid-body approach to such decay curves (Lewis et al. 1988) in which one would average curves calculated for instantaneous conformations of the particle may be rather incorrect.

3. Harvey-Wegener treatment

3.1. Instantaneous coefficients

Segmentally flexible particles have more than six degrees of freedom. Resistance and diffusion tensors Ξ and $\mathscr{D}$ of higher dimensions are defined for any instantaneous conformation of the particle, and Eq. (1) still holds. Harvey and Wegener (Harvey 1978, 1979; Harvey and Cheung 1979; Harvey et al. 1983; Wegener 1980, 1982 b; Wegener et al. 1985) proposed a treatment whose first aim is to define and calculate instantaneous, conformation dependent, Ξ and $\mathscr{D}$ tensors. The second aspect is the connection of these tensors with observable properties. This aspect was incompletely or incorrectly treated in the original work, and is one of the targets of in the present article.

There are some differences between the treatments of Harvey and Wegener. They differ initially in the choice of the coordinates that represent the degrees of freedom. Harvey uses the six coordinates for rigid translations and rotations of the particle in its instantaneous conformation, and adds the required coordinates for internal motions (bendings and torsions). Wegener uses three coordinates for rigid, center-of-mass translation plus three individual rotations for each segment. It is possible to transform $\mathscr{D}$ from one system of coordinates to the other (Harvey et al. 1983; Garcia de la Torre et al. 1985; Mellado et al. 1988). The Wegener treatment has been presented for the most general case of a particle with any number of segments, which must be allowed to undergo any type of internal motion. The treatment of Harvey has been presented for the particular case of two segments and one joint which can act either as a universal swivel, or as a hinge allowing only bending (in-plane flexing) but not torsions. Here the formalism of Wegener will be followed because it is more general.

Let us consider a general segmentally flexible particle composed by n segments connected by some number of universal swivels. One of them, labeled O, is arbitrarily chosen as a common reference. The only initial restriction on the type of particle is that the segments do not form any closed loop. The particle is diffusing freely in space, and its motion is referred to a laboratory-fixed system of coordinates. The number of degrees of freedom for n linked segments is $3n+3$. Accordingly the Ξ and $\mathscr{D}$ tensors are of dimension $(3n+3)\times(3n+3)$, and can be partitioned into 3×3 blocks in a manner similar to that shown in Eq. (2). The generalized Einstein relationship can be written now as

$$\begin{pmatrix} \mathbf{D}_{O,\mathrm{tt}} & \mathbf{D}_{O,\mathrm{tr}}^{(1)T} & \cdots & \mathbf{D}_{O,\mathrm{tr}}^{(n)T} \\ \mathbf{D}_{O,\mathrm{tr}}^{(1)} & \mathbf{D}_{\mathrm{rr}}^{(1,1)} & \cdots & \mathbf{D}_{\mathrm{rr}}^{(1,n)} \\ \cdots & \cdots & \cdots & \cdots \\ \mathbf{D}_{O,\mathrm{tr}}^{(n)} & \mathbf{D}_{\mathrm{rr}}^{(n,1)} & \cdots & \Xi_{\mathrm{rr}}^{(n,n)} \end{pmatrix}$$

$$= kT \begin{pmatrix} \Xi_{\mathrm{tt}} & \Xi_{O,\mathrm{tr}}^{(1)T} & \cdots & \Xi_{O,\mathrm{tr}}^{(n)T} \\ \Xi_{O,\mathrm{tr}}^{(1)} & \Xi_{\mathrm{rr}}^{(1,1)} & \cdots & \Xi_{\mathrm{rr}}^{(1,n)} \\ \cdots & \cdots & \cdots & \cdots \\ \Xi_{O,\mathrm{tr}}^{(n)} & \Xi_{\mathrm{rr}}^{(n,1)} & \cdots & \Xi_{\mathrm{rr}}^{(n,n)} \end{pmatrix}^{-1}. \tag{7}$$

The tt blocks correspond to the overall translational diffusivity, measured at point O. The rr blocks correspond to the rotational diffusivity of each individual segment, and the tr blocks couple translation and rotation. All the blocks are referred to the common, laboratory-fixed system of coordinates. The O subscript indicates that the corresponding block depends on the choice of O.

All the dynamic information (deterministic mobility or Brownian diffusivity) is contained in the blocks of $\mathscr{D}$, which in turn should be obtained from the blocks of Ξ. The calculation of the latter is one of the main problems of the treatment. If one wishes to include rigorously in the calculation the hydrodynamic interaction (HI) between the segments (as one should in principle), the only way is to model the segments as assemblies of beads, and the calculation of blocks of Ξ is carried out using a rather involved procedure.

The situation is simpler if one makes the approximation of neglecting hydrodynamic interaction between the subunits in the segmentally flexible macromolecule. We can make the further simplifying assumption that the segments are spheres, ellipsoids, cylinders or, in general, bodies having cylindrical symmetry. If one of such segments is free in solution, its hydrodynamics can be expressed in terms of four coefficients corresponding to translations along the symmetry axis and perpendicular to it, $f_{t,\parallel}$ and $f_{t,\perp}$, and rotations around the symmetry axis and around a perpendicular axis, $f_{r,\parallel}$ and $f_{t,\perp}$. Expressions for these coefficients are available for ellipsoids (Cantor and Schimmel 1980; Richards 1980) as well as for long and short cylinders (Tirado and Garcia de la Torre 1979, 1980, 1984; Garcia de la Torre 1989). They are all we need for the calculation of Ξ for a given conformation, as described in the next subsection. Then the components of $\mathscr{D}$ are finally calculated by numerical inversion, as indicated in Eq. (7).

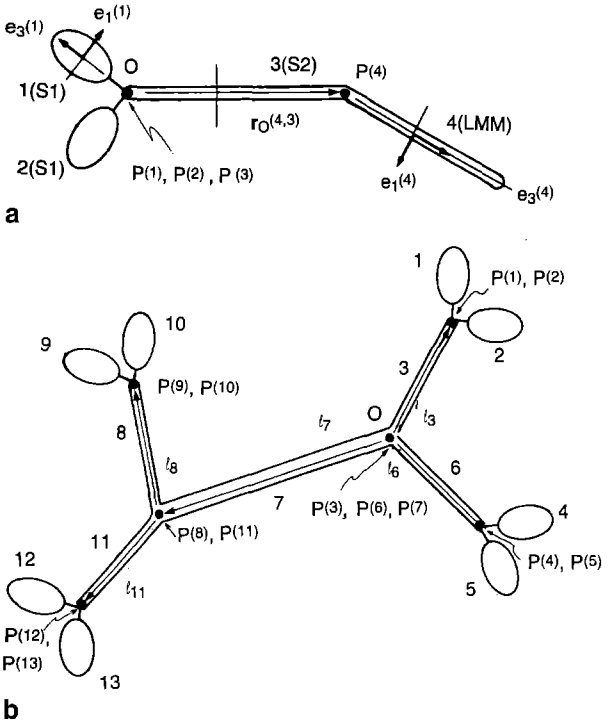

Fig. 2. **a** Schematic myosin model illustrating the vectors in the Wegener treatment. Biological notation for the subunits is indicated in parentheses. The reference joint, O, and the subunit endpoints $P^{(i)}$ are indicated. Subunit vectors $e_1^{(i)}$ and $e_3^{(i)}$ are shown for subunits 1 and 4. The only non-zero r_O^{ij}, vector, namely r_O^{43}, is shown. **b** Hypothetical model for a tetrameric myosin filament (Rau 1993), showing the placement of the O and $P^{(i)}$ points. Note length vectors for subunits 3, 6, 7, 8 and 11; the only non-zero r_O^{ij} vectors coincide with one of them (see text)

3.2. Calculation details

We summarize here the procedure for calculation of the instantaneous diffusion tensors $\mathscr{D}$ and Ξ in the Wegener coordinates, assuming first that hydrodynamic interaction between segments is neglected, and next particularizing for the case of symmetric segments (Wegener 1982b).

A particular joint, O is selected for reference. For each of the n segments, the "end-point", $P^{(i)}$, is one of the ends of the segment (actually, one of the joints linking it to the particle), which must be taken as that closest to point O. A common arbitrarily oriented system of coordinates is fixed in the laboratory. Individual systems of coordinates are also attached to each segment, with unitary vectors $e_1^{(i)}$, $e_2^{(i)}$ and e_3^i, with e_3^i along the end-to-end line of the segment, and pointing from $P^{(i)}$ to the other end. Considered as an independent body, the segment has friction tensors $\Xi_{tt}^{(i)}$, $\Xi_{tr}^{(i)}$ and $\Xi_{rr}^{(i)}$ (see Eq. (2)). Then, Wegener (1982) expresses the blocks of Ξ in the given, instantaneous conformation of the segmentally flexible particle as:

$$\Xi_{tt} = \sum_{j=1}^{n} \Xi_{tt}^{(j)} \tag{8}$$

$$\Xi_{O,tr}^{(i)} = \Xi_{P,tr}^{(i)} + \sum_{j=1}^{n} \mathbf{U}_O^{(j,i)} \cdot \Xi_{tt}^{(j)} \tag{9}$$

$$\Xi_{O,rr}^{(i,i)} = \Xi_{P,rr}^{(i)} - \sum_{j=1}^{n} \mathbf{U}_O^{(j,i)} \cdot \Xi_{tt}^{(j)} \cdot \mathbf{U}_O^{(j,i)} \tag{10}$$

$$\Xi_{O,rr}^{(i,j)} = \mathbf{U}_O^{(j,i)} \cdot \Xi_{P,tr}^{(j)T} - \Xi_{P,tr}^{(i)} \cdot \mathbf{U}_O^{(i,j)} - \sum_{m=1}^{n} \mathbf{U}_O^{(m,i)} \cdot \Xi_{tt}^{(m)} \cdot \mathbf{U}_O^{(m,j)} \tag{11}$$

where Eq. (11) holds for $i \neq j$. The matrix $\mathbf{U}_O^{ij}$ is defined as

$$\mathbf{U}_O^{(i,j)} = \begin{pmatrix} 0 & -\varrho_3 & \varrho_2 \\ \varrho_3 & 0 & -\varrho_1 \\ -\varrho_2 & \varrho_1 & 0 \end{pmatrix}. \tag{12}$$

In Eq. (12), ϱ_1, ϱ_2 and ϱ_3 are the coordinates (in the laboratory system) of a vector r_O^{ij} defined as follows: go from the endpoint $P^{(i)}$ of the $i-th$ segment to the origin O. If segment j is in the path, then $r_O^{(i,j)} = l_j$, where l_j is the length (end-to-end distance) of element j, and is directed along the end-to-end axis of j from $P^{(j)}$ to the other endpoint. Otherwise $r_O^{(i,j)} = \mathbf{0}$. By construction, $r_O^{(i,i)} = \mathbf{0}$. Also, if $r_O^{(i,j)} \neq \mathbf{0}$ then $r_O^{(j,i)} = \mathbf{0}$. Both $r_O^{(i,j)} = \mathbf{0}$ and $r_O^{(j,i)} = \mathbf{0}$ if segments i and j are on different branches or opposite sides of O. We note that Eqs. (8)–(12) are the same as Eq. (10) of Wegener (1982b) except for changes in notation and for a difference in the way of expressing cross products.

Let us consider as an example a four-segment model of the myosin molecule (Fig. 2a), with two fragments S1 ($i = 1, 2$) and one fragment S2 ($i = 3$), joined at O, and the $i = 4$ fragment, LMM, joined at the other end of S2. The $P^{(i)}$ points of the first three segments must coincide with O, and $P^{(4)}$ would be the LMM-S2 joint. Then, one finds that all the $r_O^{(i,j)}$'s are zero except $r_O^{(4,3)}$, which would be the

S2 vector. A more complex example is shown in Fig. 2b, which corresponds to a tetrameric myosin filament (Rau 1993; Rau et al. 1993). This model supposedly has 13 subunits and 6 joints. With the choice for point O made in Fig. 2b, the only non-zero vectors are

$$\begin{aligned} \boldsymbol{r}_O^{(1,3)} &= \boldsymbol{r}_O^{(2,3)} = \boldsymbol{l}_3 \\ \boldsymbol{r}_O^{(4,6)} &= \boldsymbol{r}_O^{(5,6)} = \boldsymbol{l}_6 \\ \boldsymbol{r}_O^{(9,8)} &= \boldsymbol{r}_O^{(10,8)} = \boldsymbol{l}_8 \\ \boldsymbol{r}_O^{(12,11)} &= \boldsymbol{r}_O^{(13,11)} = \boldsymbol{l}_{11} \\ \boldsymbol{r}_O^{(k,7)} &= \boldsymbol{l}_7,\ k = 8, \ldots, 13. \end{aligned}$$

The second assumption in Wegener's formalism is that the segments have symmetry of revolution. Then, the friction tensors of a segment referred its own system of coordinates (primed symbols) take simple forms. For instance, for translation

$$\boldsymbol{\Xi}_{\mathrm{tt}}^{\prime(i)} = \begin{pmatrix} f_{t,\perp} & 0 & 0 \\ 0 & f_{t,\perp} & 0 \\ 0 & 0 & f_{t,\parallel} \end{pmatrix} \tag{13}$$

where $f_{t,\parallel}$ and $f_{t,\perp}$ are the translational friction coefficients of the free segment for motions along the axis and perpendicular to it, respectively. The situation is similar for rotation, determined by coefficients $f_{t,\parallel}$ for rotation around the segment axis and $f_{t,\perp}$ for rotation around a perpendicular axis that passes through the center of the segment. The rotational friction tensor (at P) is

$$\boldsymbol{\Xi}_{P,\mathrm{rr}}^{\prime(i)} = \begin{pmatrix} f_{r,\perp} + a^2 f_{t,\perp} & 0 & 0 \\ 0 & f_{r,\perp} + a^2 f_{t,\perp} & 0 \\ 0 & 0 & f_{t,\parallel} \end{pmatrix} \tag{14}$$

and the coupling tensor:

$$\boldsymbol{\Xi}_{P,\mathrm{tr}}^{\prime(i)} = \begin{pmatrix} 0 & a f_{t,\perp} & 0 \\ -a f_{t,\perp} & 0 & 0 \\ 0 & 0 & 0 \end{pmatrix}. \tag{15}$$

In Eqs. (13)–(15), a is the distance from the midpoint of segment i to its endpoint $P^{(i)}$. It is implicitly assumed, following Wegener (1982b) that the end-to-end line coincides with the symmetry axis.

To be used in Eqs. (9)–(11), these tensors must be referred to the laboratory fixed system of coordinates. This is done pre- and post-multiplying them by the matrix $\mathbf{A}_i$ which transforms the coordinates of the segment-fixed system to the lab-fixed system:

$$\boldsymbol{\Xi}_{P,\mathrm{tr}}^{(i)} = \mathbf{A}_i^T \cdot \boldsymbol{\Xi}_{P,\mathrm{tr}}^{\prime(i)} \cdot \mathbf{A}_i. \tag{16}$$

The summary of the procedure is as follows. First, for each subunit, the two translational and the two rotational coefficients are calculated using standard formulas for ellipsoids or cylinders. Then the three friction tensors for each segment are calculated in the segment system of coordinates (Eqs. (13)–(15)) are transformed to the common system (Eq. (16)). The summations over the segments in Eqs. (8)–(11) are carried out to build the blocks of $\boldsymbol{\Xi}$ which are arranged as in Eq. (7), and finally inverted to obtain the blocks of $\mathscr{D}$.

3.3. Translational diffusion

The dependence of translational tensor, $\mathbf{D}_{O,\mathrm{tt}}$, and therefore of the macroscopic diffusion coefficient D_t, on the point O at which they are referred complicates formally the treatment of translational diffusion. On the other hand, it is well known that this property is least sensitive to modeling and theoretical refinements. While the problem of the proper reference point was unclear, it was speculated that the rigid body treatment (Harvey et al. 1983; Iniesta et al. 1988) could be a good approximation. When Wegener (1985) finally solved rigorously that problem it turned out that the rigid-body results were indeed excellent. For a completely flexible broken rod with $L/d = 20$, the rigid-body results differs only by 0.3% from the exact one, the difference being negligible in comparison with typical experimental errors. Therefore, we disregard the description of translational diffusion in the Harvey-Wegener treatment since the rigid-body treatment is perfectly valid for this property.

3.4. Rotational diffusion

The rotational diffusivity of each individual fragment, i, can be expressed in terms of the $\mathbf{D}_{\mathrm{rr}}^{(i,i)}$ tensor. As for rigid bodies, this is diagonalized to obtain the eigenvalues and eigenvectors. It turns out that one of the eigenvectors goes along the symmetry axis of the subunit, and the corresponding eigenvalue, $D_{r,\parallel}^{(i)}$, is given by

$$D_{r,\parallel}^{(i)} = k_B T / f_{r,\parallel}^{(i)} \tag{17}$$

which is the same as for the free segment. The two other eigenvalues correspond to end-over-end rotations, and depend intricately on the instantaneous geometry of the particle. For the simplest case of two subunits, the eigenvalues can be identified with rotations of the subunit within the instantaneous plane of the particle and out of it, and are denoted $D_{\mathrm{in}}^{(i)}$ and $D_{\mathrm{out}}^{(i)}$, respectively.

All this description corresponds to a particular, instantaneous conformation of the segmentally flexible particle. The observed properties will be averages over all the possible conformations, which are equally probable since, as commented above, the treatment assumes the absence of restoring forces that would restrict bending and torsion. As one would expect, $D_{r,\parallel}^{(i)}$ is independent of conformation. The two other eigenvalues are found to be close to each other for a given conformation, and their dependence on conformation is rather weak. This is illustrated for the case of a broken rod with two arms in Fig. 3. Then it seems valid to express the end-over-end diffusivity by means of a single value, $D_{r,\perp}^{(i)}$, which is the conformational average (denoted as $\langle \ldots \rangle$) of the mean of $D_{\mathrm{in}}^{(i)}$ and $D_{\mathrm{out}}^{(i)}$:

$$D_{r,\perp}^{(i)} = \langle \tfrac{1}{2}(D_{\mathrm{in}}^{(i)} + D_{\mathrm{out}}^{(i)}) \rangle. \tag{18}$$

The immediate problem is how the conformational average can be evaluated. This is easily done for the simplest case of two subunits: one would calculate the properties as a function of α, and the average is expressed as a particular case of Eq. (5) with $V = 0$

$$\langle \ldots \rangle = \tfrac{1}{2} \int_0^{\pi} (\ldots(\alpha)) \sin\alpha \, \mathrm{d}\alpha. \tag{19}$$

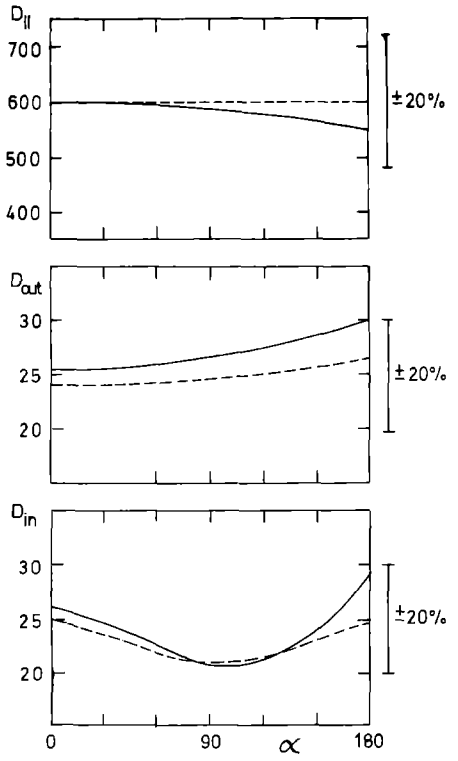

Fig. 3. Instantaneous values of the rotational coefficients $D_{\|}$, D_{in} and D_{out} of the two identical arms of a broken rod with length-to-diameter ratio, $L/a = 20$, versus the angle between arms, α. Results from Mellado et al. (1988), with hydrodynamic interaction (HI) (*continuous curves*) and without HI (*dashed curves*). The specific unit used for the coefficients is irrelevant; note essentially the magnitude of the HI effect and the α-dependence. A $\pm 20\%$ bar centered at the no-HI value for $\alpha = 0$ is displayed

For more complex particles, Wegener describes a method to select a few representative conformations, which would be the only ones included in the averaging. His method has the disadvantage of being formally complex and difficult to program. As the time required for evaluating one conformation is so short in present computers, one could think of an alternative procedure in which a sample containing a moderate number (a few hundred) conformations is generated by simple Monte Carlo procedures, and the average is carried our over the sample. This idea has been applied in the calculation of the radius of gyration (Solvez et al. 1988).

The perpendicular, end-over-end rotational diffusion coefficient, and all the individual values of which it is the average, have the interesting property of being bracketed by two bounds, $D^{(i)}_{fixed}$ and $D^{(i)}_{free}$ as

$$D^{(i)}_{fixed} \leq D^{(i)}_{r,\perp} \leq D^{(i)}_{free}. \tag{20}$$

The upper bound is the end-over-end rotational diffusion of the subunit if it were free in solution, given by $D_{free} = k_B T / f_{r,\perp}$. The lower bound corresponds to rotation with one of the ends fixed, and is given by $D_{fixed} = k_B T / (f_{r,\perp} + a^2 f_{t,\perp})$, in terms of quantities defined in subsection 3.2. If one subunit in a segmentally flexible macromolecule is much larger that the rest, it will dominate the rotational behavior with a $D_{r,\perp}$ very close to D_{free}. In contrast, if the subunit is much smaller than the rest of the molecule, its $D^{(i)}_{r,\perp}$ will be close to $D^{(i)}_{fixed}$ if it is terminally anchored (Iniesta and Garcia de la Torre, 1987).

Now, according to Wegener (1982b), the contribution of the subunit i to the property whose dynamics is being observed will involve three relaxation times, which are given by the same expression as for a free axially symmetric body, in terms of the $D^{(i)}_{r,\|}$ and $D^{(i)}_{r,\perp}$ coefficients so calculated:

$$\tau^{(i)}_a = 1/6 D^{(i)}_{r,\perp} \tag{21}$$

$$\tau^{(i)}_b = 1/(D^{(i)}_{r,\|} + 5 D^{(i)}_{r,\perp}) \tag{22}$$

$$\tau^{(i)}_c = 1/(4 D^{(i)}_{r,\|} + 2 D^{(i)}_{r,\perp}). \tag{23}$$

For a macromolecule composed of identical, equivalent segments the (i) index can be suppressed. If the electro-optic or spectroscopic properties of the subunit have axial symmetry, the only relevant relaxation time will be the longest one (Eq. (21)) hereafter indicated as τ_{HW}. In the case on non-identical subunits, there will be one $\tau^{(i)}_{HW}$ for each of them.

3.5. Hydrodynamic interaction effects

As described above, the original Harvey-Wegener treatment neglects hydrodynamic interactions between subunits (but not within each subunit). If one wishes to include rigorously in the calculation the hydrodynamic interaction (HI) between the segments (as one should in principle), the only way is to model the segments as assemblies of beads (this is so because HI between nonspherical elements is enormously complicated).

Essentially, most of the aspects of the Harvey-Wegener treatment described so far are valid with HI. The HI effects are considered at the beginning of the procedure, in the calculation of the components of the friction tensors, Ξ_{tt}, $\Xi^{(i)}_{P,tr}$ and $\Xi^{(i)}_{P,rr}$. Instead of the simple forms described in Eqs. (13)–(16), in the HI case these tensors are calculated using more complex equations that can be found in the literature (Wegener 1982a; Garcia de la Torre et al. 1995; Mellado et al. 1988). The rest of the procedure is identical to the no-HI case.

The HI effect can be tested with bead models switching off the HI between beads belonging to different subunits, comparing the results with those for the case with HI between every pair of beads. Some illustrative results are described in Table 1. We note that the translational diffusion coefficient, D_t, is remarkably influenced by HI; when this effect is neglected, the error in D_t may be up to 40%. The Harvey-Wegener treatment without HI should not be applied, therefore, for the calculation of D_t. Alternatively, D_t can be evaluated using the simple, rigid-body treatment which, as discussed above, is nearly exact for this property.

On the other hand, the HI effect is rather less important in the case of rotational coefficients. For $D_\perp$, wich determines the longest relaxation time (Eq. (21)), the error is about 20% for compact structures, and smaller for more open structures made up of elongated segments, such as a long broken rod or a myosin molecule. Further-

Table 1. Ratios $D(\text{no HI})/D(\text{HI})$ for various diffusion coefficients

	D_t	$D_\perp$	$D_\parallel$
Broken dumbbell[a]	0.82	0.87	1.00
Trumbbell[b]	0.52	0.75	1.00
Short broken rod[c]	0.72	1.02	1.04
Long broken rod[d]	0.76	0.93	1.02

[a] Bead radii $\sigma = 0.25$; distance from joint to bead center $b = 1$. (Garcia de la Torre et al. 1985)
[b] Two beads at ends and one bead at the hinge, with $\sigma = 0.5$ and $b = 1$. (Harvey et al. 1983; Diaz and Garcia de la Torre 1988)
[c,d] Rods with $L/a = 4$ and 20 modeled with 4 and 20 touching beads, respectively, half of them at each arm (Wegener 1982; Mellado et al. 1988).

more, $D_\parallel$ is practically the same with and without HI, so that the errors in the two other relaxation times that contain $D_\parallel$ are neglectable. Thus, we arrive at an important conclusion in this regard: The effect of neglecting HI, which is one of the main drawbacks of the simplest version of the Harvey-Wegener treatment, is quite small in the case of rotational diffusion.

3.6. In-plane bending

As presented so far, the Harvey-Wegener treatment requires that the joints in the segmentally flexible molecule act as universal swivels, allowing unrestricted bending and torsions. There is a variation of the theory for a different, special case, in which torsions are forbidden and only free bending is allowed (Harvey 1979; Harvey et al. 1983; Wegener 1980). The formalism has been worked out only for macromolecules with two subunits, such as the broken, hinged rod. (We prefer to reserve the hinged qualifier for this special case.) Instead of the nine degrees of freedom of the swivel-jointed rod, the hinged rod has only seven, of which six are those proper for a rigid particle, and the remaining one is that corresponding to bending in the particle's plane.

Mellado et al. (1988) have shown that the D_{in} coefficient of the hinged rod is the same as that for the swivel-jointed rod. However, D_{out} differs appreciably, and is not nearly constant as in Fig. 3, but instead shows a strong dependence on conformation. Finally, $D_\parallel$ is much smaller for the hinged rod. This can be understood noting that, in the hinged rod, the rotation of one arm around its own axis requires that the other rotates in space describing a cone, within the subsequent increase in friction and decrease in diffusion.

In short, the case of restricted or forbidden torsion adds further difficulties and it should not be treated by means of the Harvey-Wegener treatment.

4. Brownian dynamics simulation

When existing theories of macromolecular dynamics are somehow unsatisfactory, one has the remedy of simulating in the computer the Brownian behavior of macromolecular models. The Brownian Dynamics (BD) simulation technique was pioneered by Ermak and McCammon (1978) and some of the first applications were made precisely for semiflexible macromolecules (Allison and McCammon 1984a, 1984b; Diaz et al. 1987; Diaz and Garcia de la Torre 1988). A number of applications of BD for segmentally flexible and wormlike macromolecules have been published in the last five years. The description of the BD technique would merit a separate review, and it is outside the scope of the present paper. A succinct summary of the procedure is presented here, and in the next section its particular applications to the present problem will be discussed.

The models for BD simulation are bead models such as those described above. In the case of segmentally flexible macromolecules, each subunit is represented by one bead or by an array of beads. Rigid constraints or quasi-rigid connectors hold together the beads within a given subunit to preserve its rigid shape. The semiflexible joints are usually represented by a single bead that keeps the subunits connected but allows some degree of flexibility, characterized by the variability of the angle α between the subunit axes. Usually, a bending potential of the type $V/k_BT = Q(\alpha - a_0)^2$ is assumed, where α_0 is the equilibrium value of the intersubunit angle (see Fig. 1) and the constant Q gauges the flexibility of the joint.

The Brownian dynamics of such models are simulated from the very first principles of Brownian motion, which are implemented in an algorithmic procedure. The position each bead in the particle, $\boldsymbol{r}_k\,(k = 1, \ldots N)$, after a time step, Δt, is obtained from the initial position, $\boldsymbol{r}_k^0$, as:

$$\boldsymbol{r}_k = \boldsymbol{r}_k^0 + \frac{\Delta t}{k_BT}\sum_{l=1}^{N}\mathbf{D}_{kl}^{\prime 0}\cdot\mathbf{F}_l^0 + \Delta t\sum_{l=1}^{N}\left(\frac{\partial \mathbf{D}_{kl}^{\prime}}{\boldsymbol{r}_k}\right)^0 + \mathbf{R}_k(\Delta t) \tag{24}$$

in terms of the forces $\mathbf{F}_l^0$ acting on each bead, the diffusivities $\mathbf{D}_{kl}^0$ of the multi-bead system (eventually including HI) and the random displacements, $\mathbf{R}_k(\Delta t)$ that are characteristic of Brownian motion. Initially the Ermak-McCammon (1978) algorithm was used, and recently a more efficient modification of the former has been developed (Iniesta and Garcia de la Torre 1990). The repetitive use of the algorithm generates a Brownian trajectory, i.e. a time series of positions of each bead in the particle. From the trajectory, experimentally observed properties such a transient birefringence, dynamic light scattering and fluorescence depolarization can be simulated. This usually involves correlation functions or similar forms, $C(t)$, of the type

$$C(t) = \langle F(t_0, t_0 + t)\rangle_{t_0} \tag{25}$$

$F(t_0, t_0 + t)$ is a function of the positions of the particle at instants t_0 and $t_0 + t$, which is averaged over the choice of the initial along the trajectory. The result is function of the elapsed time, t, which is usually fitted to a single or multiple exponential decay:

$$C(t) = a_1 \exp(-t/\tau_1) + a_2 \exp(-t/\tau_2) + \ldots . \tag{26}$$

The a_i coefficients, and essentially the rotational relaxation times, τ_i, are the primary results of the simulation. In addition to their comparison with experimental data,

these results, and particularly the longest relaxation time τ_1 and the initial relaxation time,

$$\tau_{ini} = (a_1 \tau_1^{-1} + a_2 \tau_2^{-1} + \ldots)^{-1} \quad (27)$$

can be used to check the performance of theoretical approaches such as the rigid-body and the Harvey-Wegener treatments.

Simple examples of correlation functions are those for which the F function is of the form $P_2(\cos\theta_v) \equiv (3\cos^2\theta_v - 1)/2$, so that

$$C_v(t) = \langle P_2(\cos\theta_v(t_0, t_0 + t))\rangle_{t_0} \quad (28)$$

where θ_v is the angle subtended by two orientations of some vector, v, at times t_0 and $t_0 + t$. Such a vector can be the end-to-end vector, in the case of non-branched structures. It can also be a vector along the main axis of any of the segments in the molecule, and then the correlation function is related to the fluorescence anisotropy decay for a probe attached to that particular segment. There are other, more involved correlation functions, related to electric birefringence, depolarized and polarized dynamic light scattering (Allison 1986; Allison et al. 1990; Allison and Nambi 1992) and viscoelasticity (Diaz et al. 1990).

5. Simple models

We now present results for two particularly simple models of segmentally flexible macromolecules, namely the trumbbell and the broken rod. These models have been thoroughly studied using both the theoretical approaches (rigid-body treatment and the Harvey-Wegener formalism) as well as the simulation technique. We describe only the general, qualitative aspects of the results, that are expected to be valid for any segmentally flexible macromolecule.

5.1. The trumbbell

The semiflexible trumbbell (Hassager 1974; Roitman and Zimm 1984a, b) is depicted in Fig. 1. It consists of three beads joined by two practically rigid connectors. The central bead acts a semiflexible joint, allowing restricted bending with an associated potential energy, as described above, given by $V = k_B T Q (\alpha - \alpha_0)^2$, where α_0 is the equilibrium angle ($\alpha_0 = 0$ for the straight conformation), and Q is a dimensionless rigidity constant, with $Q = 0$ for the completely flexible model, and $Q \to \infty$ for the rigid case. Usually one takes $\alpha_0 = 0$, but semiflexible bent trumbbels have also been considered (Roitman, 1984).

A number of theoretical results using various treatments (Harvey et al. 1983; Roitman and Zimm 1984a, b; Nagasaka and Yamakawa 1985) and results from BD simulation (Diaz and Garcia de la Torre 1988, 1994; Garcia de la Torre et al. to be published) are available. This allows a precise assignment of the differential relaxation times and other properties predicted by the theories to the various observable dynamic properties, in different time scales.

A simple but relevant case is that of translational diffusion. In Fig. 4 we plot values of the D_t coefficient obtained

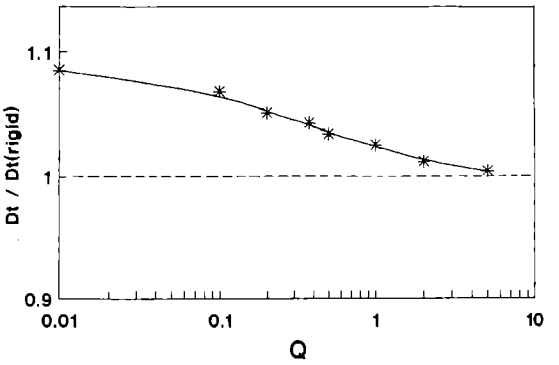

Fig. 4. Translational diffusion coefficients of trumbbells with varying rigidity Q, normalized to the value for the completely rigid and straight structure. The continuous line represents results from the rigid-body treatment. The data points are BD simulation results

with the rigid body approximation, along with BD simulation results calculated from the mean-square displacement of the center of mass through the Einstein formula, $\langle r_{cm}^2 \rangle = 6 D_t t$ which (apart from statistical errors in the simulation) is free of any approximation. It is clear that the rigid body treatment performs very well for translational diffusion. This is in part due to the low sensitivity of this property to conformation; in the case shown here, D_t changes less than 10% from the most flexible structure to the most rigid one. Thus, the present example makes it clear that the rigid-body treatment is completely adequate for translational properties such as the translational diffusion and the sedimentation coefficients.

The BD results for rotational correlation functions, analyzed in terms of a multiexponential decay with different relaxation times, can be compared with the relaxation times predicted by the rigid-body and the Harvey-Wegener treatments. Here we do so for three correlations functions:

- $C_e(t)$, of the type of Eq. (28) for the reorientation of the end-end vector, r_{13}
- $C_b(t)$, of the type of Eq. (28) for the reorientation of any of segments or bond vectors, r_{21} or r_{23}
- $C_d(t)$, for depolarized dynamic light scattering (DDLS), which is also valid for transient electric birefringence of a molecule with permanent dipole moments (see Allison 1986; Allison and Nambi 1992).

The functions are normalized so that at zero time, $C(0) = 1$.

A plot of these functions (not shown) for the most flexible model, with $Q = 0$ shows a salient feature: the segment and DDLS functions, $C_b(t)$ and $C_d(t)$, are nearly coincident over two decades of decay. These decays are essentialy monoexponential, with a correlation time that turns out to be equal to the Harvey-Wegener longest relaxation time, τ_{HW} (Eq. (21)). On the other hand, the end-to-end function $C_e(t)$ seems to decay at long times with a relaxation time equal to the rigid-body value, except for the behavior at short times. Indeed, the initial behavior (at very short times) of the all three functions, shown in Fig. 5, follows the same rate, given by τ_{HW}^{-1}. For an intermediate rigidity, $Q = 0.5$, the full decay curves are presented in Fig. 6, which illustrates well the meanings of the

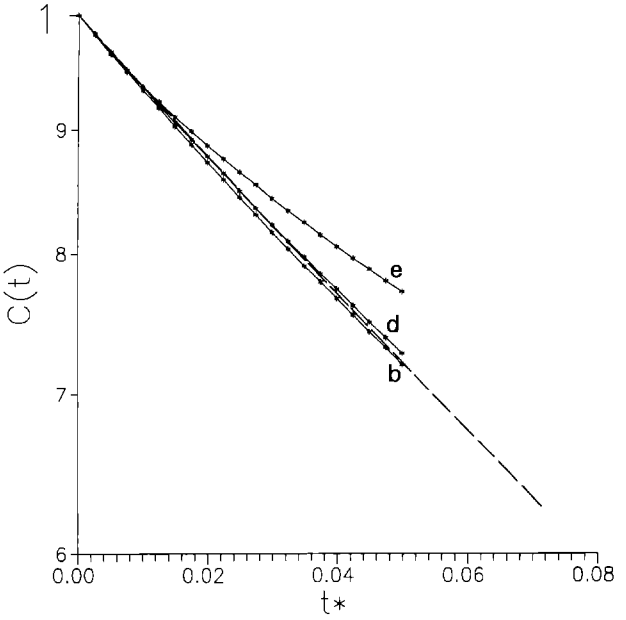

Fig. 5. Short-time behavior of the correlation functions $C_e(t)$ (*e*), $C_b(t)$ (*b*), and $C_d(t)$ (*d*) for $Q=0$. Time is in arbitrary units. The discontinuous line marks the initial slope of the three curves, equal to τ_{HW}^{-1}

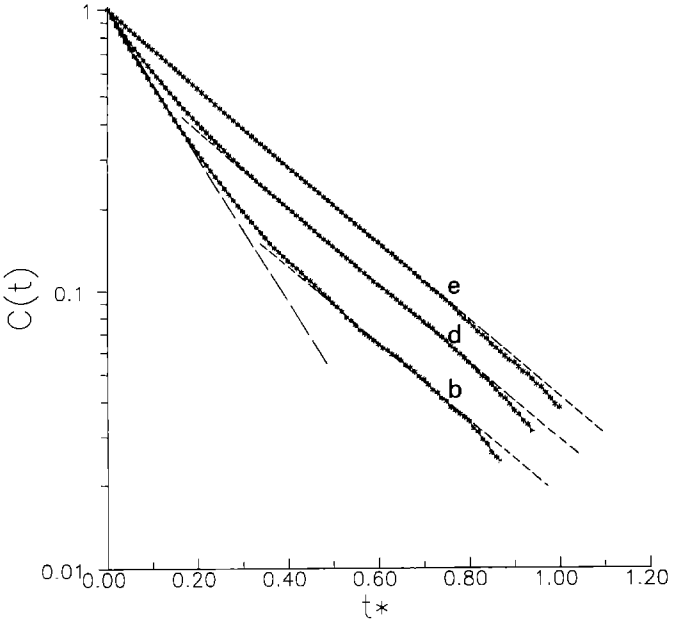

Fig. 6. Long-time behavior of the correlation functions $C_e(t)$ (*e*), $C_b(t)$ (*b*), and $C_d(t)$ (*d*) for $Q=0.5$. Time is in arbitrary units. The discontinuous lines mark the initial slope of the three curves, equal to τ_{HW}^{-1} and the final slope, equal to τ_{rb}^{-1}

two relaxation times: at long times, all the decays follow a rate equal to τ_{rb}^{-1}, while at short times the decay rate is τ_{HW}^{-1}. For very rigid trumbbells, most of the decay is dominant by τ_{rb}; the initial region is hardly noticed.

The parameters that can be most precisely determined from the decays are the longest relaxation time, τ_1, and its corresponding amplitude, a_1. These results are plotted in Fig. 7 for trumbbells of varying flexibility. For the various

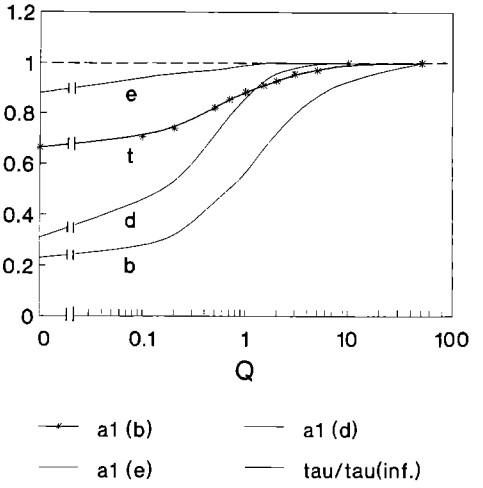

Fig. 7. Longest relaxation time $\tau_1(t)$ and its amplitude in $C_e(t)$ (*e*), $C_b(t)$ (*b*), and $C_d(t)$ (*d*). The data points are τ_1 values normalized to the value for the $Q\to\infty$ limit The (*t*) curve is the prediction from the rigid-body treatment

decays, τ_1 is the same and coincides with the calculated τ_{rb}. However, the relative amplitude varies remarkably from one property to other. For instance, for $Q=1$, τ_{rb} determines the whole $C_e(t)$ decay, while it only contributes 86% and 56%, to $C_d(t)$ and $C_b(t)$, respectively.

5.2. The broken rod

The broken rod is a paradigmatic case of a segmentally flexible macromolecular model. Since the pioneering work of Yu and Stockmayer (1967), this model has received continuing attention; the successive developments for rigid and semiflexible macromolecules have been customarily applied to broken rods. The interest in the model is twofold. From the experimental point of view, it can be representative of a variety of biopolymers, such as the myosin rod (Harvey and Cheung 1982) or hinged synthetic polypeptides (Matsumoto et al. 1975). Theoretically, the broken rod is simple and useful to characterize deviations from the straight-rod behavior.

The broken rod has a diameter d and a total length L, which is divided into two arms of lengths L_1 and L_2. The maximum deviations from the rigid, straight rod, take place for the symmetric case with $L_1=L_2$, which will be the only one shown hereafter. As for the trumbbell, the bending potential is assumed to be quadratic in the departure of the α angle from the equilibrium value α_0 (usually $\alpha_0=0$). Thus the potential is given by $V=k_BTQ(\alpha-\alpha_0)^2$ where Q is the rigidity constant.

Equilibrium properties of the broken rod are calculated using the rigid-body treatment. This includes not only the radius of gyration but also other properties such as the Kerr constant, which determines the static birefringence in an electric field (Frederick and Houssier 1973; Mellado and Garcia de la Torre 1982; Iniesta and Garcia de la Torre 1989). As noted above, the rigid-body treatment is reasonably valid for overall dynamic properties such as the translational diffusion coefficient, D_t, the in-

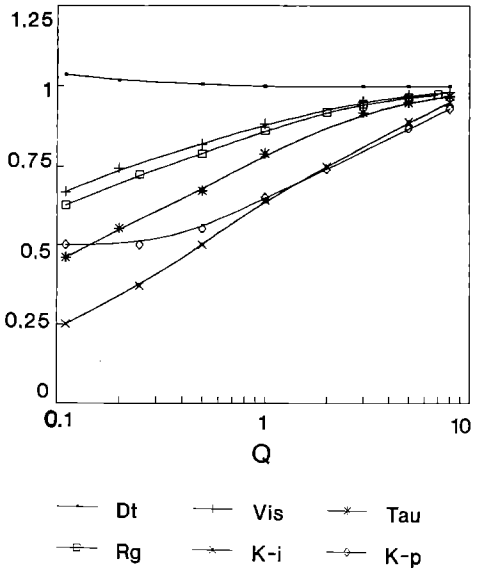

Fig. 8. Variation of the properties of semiflexible rods of equals arms with the rigidity parameter Q. The plotted values are actually the ratios property $(Q\to\infty)$/property (Q), and correspond to $L/d=48$ although, for all the properties these ratios change very slowly with L/d. Key for properties: D_t, translational diffusion coefficient; R_g, root-mean-square radius of gyration; $[\eta]$, intrinsic viscosity; Tau, relaxation time; $K-i$, specific Kerr constant for induced dipole; $K-p$, the sane, for permanent dipole

trinsic viscosity, $[\eta]$, and a relaxation time τ_{rb}. The influence of the partial flexibility of the rod in these properties is illustrated in Fig. 8 (Iniesta et al. 1988; Iniesta and Garcia de la Torre 1989). It is interesting to note that, of the two equilibrium properties, the Kerr constant is the one that changes most on going from the rigid limit to the completely flexible one. In regard to the dynamic properties, it is evident that D_t is extremely insensitive to flexibility (as noted for the trumbbell), while the τ_{rb} relaxation time presents the largest variations. The ratio of the values for totally rigid $(Q\to\infty)$ and totally flexible $(Q=0)$ rods, is $\tau_{rb}^{\text{rigid}}/\tau_{rb}^{\text{flexible}}\approx 2$. This was semiquantitatively predicted by Yu and Stockmayer (1967).

The Harvey-Wegener treatment can be easily applied to the broken rod, calculating the characteristic relaxation time τ_{HW}. Wegener (1980) reported $\tau_{\text{HW}}^{\text{rigid}}/\tau_{\text{HW}}^{\text{flexible}}\approx 4$, in apparent disagreement with the Yu-Stockmayer prediction. Hydrodynamic interaction between arms is not responsible for the difference, as its influence on τ_{HW} is about 10% (Wegener 1982a). Brownian Dynamics simulation have been used to clarify this discrepancy (Iniesta et al. 1991; Garcia de la Torre et al., in preparation). Figure 9 shows the decay of $C_a(t)$ for broken rods of varying flexibility ($C_a(t)$ for the broken rod is equivalent to $C_b(t)$ for the trumbbell; now the pertinent vector is that going from the joint to the end of the arm). At long times, the decay rate (slope in the semilogarithmic plots) is greater for greater Q, reflecting the larger overall size of the particle. However, at the very beginning of the decay, all the curves show the same initial slope. Figure 10 displays three decay functions for the same rod, with $Q=0.5$. For the three properties, the final decay rate is the same and

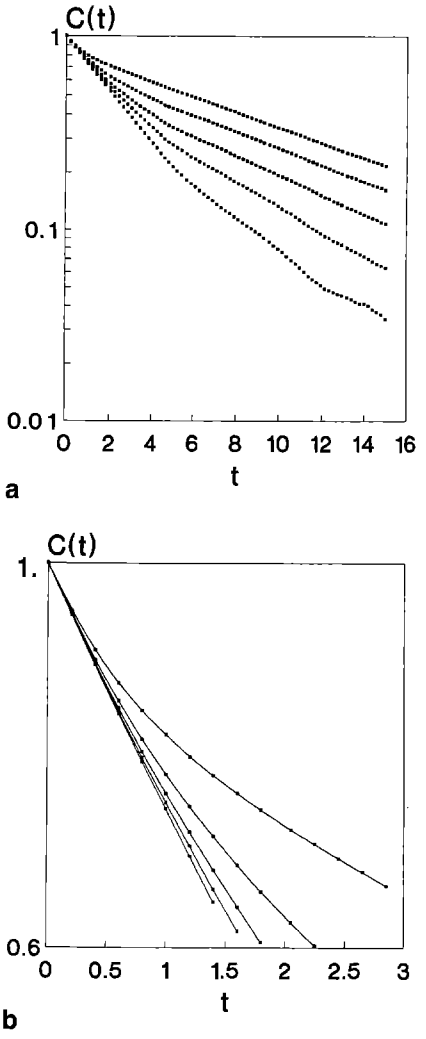

Fig. 9. a Decay function $C_a(t)$ for broken rods with $L/d=11$ and equal arms, plotted versus reduced time t^*. Curves from bottom to top correspond to $Q=0$, 0.5, 1, 2 and 5. **b** Short time behavior of the same decays

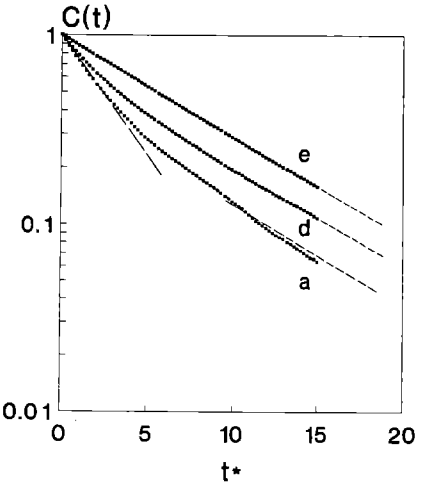

Fig. 10. Decay functions for three properties: arm vector $C_a(t)$ (*a*), end-to-end vector, $C_e(t)$ (*e*), and depolarized dynamic light scattering, $C_d(t)$ (*d*), for $Q=0.5$. The slope and the long-dashed and short-dashed lines are, respectively, τ_{HW}^{-1} and τ_{rb}^{-1}

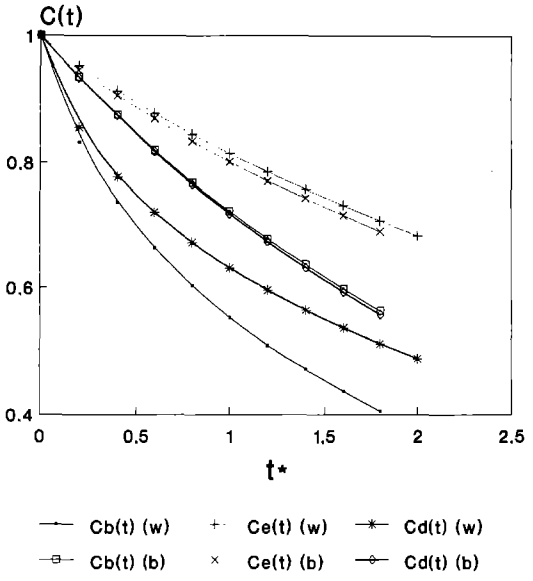

Fig. 11. Decay functions for a broken rod with $L/d = 11$ and $Q = 0$ and a wormlike rod with the same L/d and a persistence length such that the radius of gyration is the same for the both models

coincides with τ_{rb}, while the initial decay rate is, in the three cases, coincident with τ_{HW}.

Other properties of broken rods, such as dynamic light scattering (Zero and Pecora 1982; Moro and Fujiwara 1986) and rheological behavior (Jorquera et al. 1990), have been calculated theoretically. It is hoped that Brownian Dynamics will be soon extended to these properties, in order to verify the theoretical predictions.

Although the case of wormlike macromolecules is outside the scope of this article, it is interesting to include here a comparison between broken and wormlike rods. Conformational and overall properties of the two models have been analyzed comparatively (Garcia Molina and Garcia de la Torre 1984), and the comparison has been now extended to decay functions (Garcia de la Torre, in preparation). Figure 11 shows three decay functions for the freely hinged rod ($Q = 0$) and a wormlike rod having the same contour length, L, and the same radius of gyration. Thus, the longest relaxation times τ_1 are very similar for the two models. However, the initial decay for the central bond vector, and for depolarized dynamic light scattering, are remarkably faster for the wormlike rod. Indeed, for the particular case in Fig. 11, τ_{ini} is about twice as short for the wormlike model as for the broken rod. This may open an efficient way to ascertain the flexibility mechanism of semiflexible macromolecules.

5.3. General consequences

The comparison of the relaxation times calculated from the rigid-body treatment, with the decay functions for various properties, suggest the following general conclusions:

1. τ_{rb} determines the long-time decay rate of all the studied properties, coinciding therefore with τ_1. Its value depends on the degree of flexibility.

2. τ_{HW} determines the initial decay rate of all the studied properties, and coincides therefore with τ_{ini}. Although in the Harvey-Wegener treatment the particle is assumed to be freely jointed, this seems to be valid for any degree of flexibility.

3. The relative contributions of the various components in the decays (coefficients a_i in Eq. (26)) depend strongly on the degree of flexibility, and vary from one property to an other. It may happen that the amplitude of the slower component is small and most of the decay is dominated by τ_{HW}. The opposite may also happen, and in such a case the whole decay will be governed by τ_{rb}. These alternatives must be taken into account when comparing experimental data for two or more properties, and in the comparison with the theoretical predictions.

4. Different flexibility models with the same overall dimensions have quite similar values of τ_1 but quite different values of τ_{ini}. This might be useful to ascertain the flexibility mechanism (continuous or discontinuous) of semiflexible macromolecules.

6. Two typical systems

6.1. Antibodies

It has been assumed that the immunological function of antibodies is related to the partial flexibility of the immunoglobulin molecules. These macromolecules have three well-defined subunits, two F_{ab} and one F_c fragment, connected by a single joint so that the structure looks like to a T or a Y letter. From the earliest works, this joint was supposed to act as a semiflexible hinge, allowing internal motions of the fragments; actually the term "segmentally flexible macromolecule" was coined by Stryer and coworkers (Yguerabide et al. 1970) in their pioneering study of fluorescence anisotropy decay of immunoglobulins. The fluorescence decay for a probe attached to one of the three arms of the molecule must depend, in addition to the overall rotational diffusivity, on the internal mobility of the arms. In later studies, the technique was applied to a variety of native and genetically engineered antibodies to characterize their varying flexibility (Oi et al. 1984; Dangl et al. 1988).

In an attempt to correlate the observed anisotropy decay with internal semiflexibility, we carried out a Brownian Dynamics simulation study of one of the supposedly most flexible species, the human immunoglobulin IgG1 (Diaz et al. 1990). The model was extremely simple: it just consists of four spheres, three for the two F_{ab} and the F_c fragments, and a small one representing the hinge (see Fig. 12). The spheres are joined by quasirigid connectors. The partial flexibility of the molecule is associated with an intramolecular potential that is simply expressed (by analogy to the trumbbell) as:

$$V = k_B T \sum_{i=1}^{3} Q(\alpha_i - \alpha_{i,0})^2 \tag{29}$$

where the α_i's are the three interarm angles, whose equilibrium values are taken to be $\alpha_{i,0} = 120°$. As for the trumbbell, Q is a dimensionless rigidity constant, with the

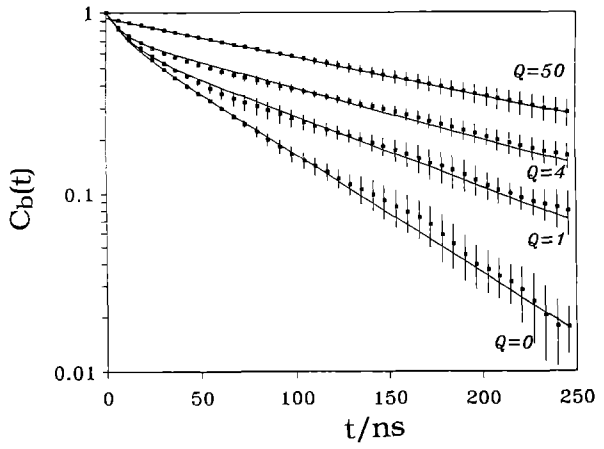

Fig. 12. $C_b(t)$ functions simulated for the immunoglobulin model with the indicated values of the rigidity parameter Q. Here time is employed in physical units. The continuous lines are double-exponential fits, with the parameters listed in Table 2

Table 2. Model parameters and simulation results for immunoglobulin

Model parameters				
Bead number, i	1	2	3	4
Radii, σ_i, nm	2.44	2.44	2.56	0.44
Connectors/angles, j		1	2	3
Connectors, b_j, nm		6.1	6.1	5.8
Equilibrium angles, $\alpha_{0,j}$, degrees		120	120	120

Overall properties					
		Rigid model ($Q\to\infty$)		Flexible model ($Q=0$)	
Exptal		RB	BD	RB	BD
R_g, nm	6.0	6.3	6.3	5.7	5.0
D_t, 10^7 cm^2/s	4.25	4.23	4.30	4.50	4.79
$[\eta]$, cm^3/g	6.2	6.5		5.7	

$C_b(t)$, Brownian dynamics				
	$Q=50$	$Q=4$	$Q=1$	$Q=0$
a_1	0.935	0.746	0.681	0.780
τ_1 (exptal: 100 ns)	202	151	109	64
τ_2		8	11	9

limits $Q\to\infty$ for the case of a rigid, Y-shaped molecule, and $Q=0$ for the completely flexible structure. In addition, a repulsive potential between the spheres was added to avoid unphysical overlapping during the simulation.

The model parameters were taken from approximate dimensions of the immunoglobulin molecule, using also literature values for the volume and solution properties of the subunits. Thus the set of parameters listed in Table 2 was selected. Before BD simulation, a preliminary rigid body calculation was carried out in order to test the model parameters by comparing rigid-body results for overall properties with experimental data. Then BD trajectories were simulated, from which new results for the overall properties were extracted. It is clear from Table 2 that experimental values are well bracketed by the two limits of flexibility, suggesting the semiflexible nature of the molecule.

The experimental fluorescence decay was associated with the simulated decay of $C_b(t)$, were the pertinent "arm" vector is that going from the hinge to the center of one of the extreme beads. It may happen that the transition moment vectors do not coincide with this axial direction. However, in any case, the longest relaxation time of $C_b(t)$ is comparable with the experimental one. Figure 12 shows $C_b(t)$ functions for varying flexibility, from which the relaxation times listed in Table 2 were extracted. The experimental value, of about 100 ns, is again well within the two limiting cases. Regarding Q as an adjustable parameter, a best fit between experiment and BD predictions is obtained for $Q\approx 1$. The amount of internal motion allowed by this partial flexibility is enough for the assumed role of the molecule in immune processes (Diaz et al. 1990).

In a subsequent work, Diaz et al. (1993) used BD simulation to predict a non-dynamic property, the solution x-ray scattering diagram, for the particular case of immunoglobulin models. In this case, BD serves as a procedure to sample the conformational space of the molecule, thus illustrating another application of the simulation techniques for segmentally flexible macromolecules.

6.2. Myosin and its fragments

As commented above, myosin and the myosin rod fragment are typical (and controversial) cases of applicability of the theories for segmentally flexible macromolecules. Indeed, much experimental and theoretical effort has been devoted to detect the possible flexibility at the joint between the heads (S1 subfragments) and the rod, and, more importantly, at the region connecting the two subfragments (S2 and LMM) that make the myosin rod. While some works suggest that there may be a fairly large flexibility within the rod (Highsmith et al. 1982; Cardinaud and Bernengo 1985; Iniesta et al. 1988), others indicate that the rod is nearly rigid (Hvidt et al. 1982, 1984; Curry and Krause 1991). Even if the rod is somewhat flexible, it is not clear whether flexibility is localized at a hinge or distributed along the rod contour, as in a wormlike rod. Thus the problem of myosin flexibility is not solved as yet, and this is mainly due to three reasons:

a) The length of the rod, which is a sensitive parameter needed for the modeling or analysis of experimental results, is not conclusively determined. A length of 144 nm is often quoted, but other values as large as 156 nm have been assumed by some workers.

b) Remarkable discrepancies between different laboratories have been published, regarding essentially the rotational relaxation times. The differences arise from sample preparation and handling as well as from fitting of the observed decays (Cardinaud and Bernengo 1985; Hvidt et al. 1984; Curry and Krause 1991).

c) Two different theoretical treatment have been applied: the rigid-body procedure (Garcia de la Torre and Bloom-

field 1980; Iniesta et al. 1988), and the Harvey-Wegener formalism (Wegener 1982b). As is emphasized in the present review, the different relaxation times resulting from the two approaches have different physical meanings and are valid in different situations. This circumstance was unknown in the previous analyse of experimental results.

Two useful properties that can be safely analyzed in terms of the rigid body treatment are R_g and $[\eta]$. In Table 3 we collect experimental values of these properties and the longest relaxation time, $[\eta]$. Data are taken from previous compilations (Garcia de la Torre and Bloomfield 1981; Iniesta et al. 1988), with the addition of some newer values (Hvidt et al. 1984; Curry and Krause 1991). These values are compared with those calculated for assuming a rigid, straight rod, with various choices for the length. If the rod is partially flexible, the experimental R_g and $[\eta]$ should be smaller than the results calculated for the rigid rod. We find that this is indeed the case, more noticeably for the isolated rod than for whole myosin, even for the shortest length. If the rod length were 156 nm, the amount of flexibility required to fit the experimental data would be quite large. In brief, there is evidence that the myosin rod has a considerable flexibility. Taking $L = 150$ nm, the results for myosin, rod can be fitted with Q values that depend slightly on the property, with an average of $Q \approx 0.5$.

Table 3 also lists the calculated τ_{rb}, which should be associated to the experimental τ_1. On the other hand, the Harvey-Wegener treatment can applied to the myosin rod and two whole myosin to assign relaxation times, τ_{HW}, to each subunit (Wegener 1982b). Examples of the results are given in Table 4. We recall from our previous discussion of HI effects between different subunits that the inclusion of such effects would lower τ_{HW} by roughly 10%.

Commonly accepted experimental values for the longest τ_1 had been 26 μs for the myosin rod and 38 μs for whole myosin (see Iniesta et al. 1988). These values are more or less (depending on length choices) smaller than the theoretical predictions for a straight, rigid rod, which had been interpreted in terms of some flexibility within the rod. Recently, Curry and Krause (1991) have questioned the previous experimental value for whole myosin, claiming that a careful analysis of birefringence decay reveals two exponentials. The slower component has $\tau_1 = 50$ μs, and the faster one has $\tau_2 = 1$ μs, with normalized amplitudes $a_1 \approx 2/3$, and $a_2 \approx 1/3$. The new estimate, $\tau_1 = 50$ μs is very close to the predictions for a straight rigid rod (Tables 3 and 4). On the other hand, the biexponential form of the decay is clearly indicative of flexibility, although not necessarily only in the rod, since some contribution may come from a semiflexible attachment of the heads.

It is interesting to note in Table 4 that for the myosin heads, $\tau_{HW} \approx 0.26$ μs, one or two orders of magnitude smaller than the relaxation times of the two other subunits. If the myosin heads were rigidly attached to the molecule, the observed relaxation time in the fluorescence decay of a probe fixed to a head would be of the order of τ_{rb}, say 40–50 μs. However, the experiments (Pads et al. 1984; Kinosita et al. 1984; see Wegener 1982b for earlier data) show the opposite: most of the decay is determined by a relaxation time of 0.2–0.3 μs quite similar to τ_{HW}. This suggest that the head-rod joint is remarkably flexible. Thus, the hydrodynamic approach described here produces information complementary to, high-resolution X-ray studies that are being recently applied to myosin structure and function (Rayement et al. 1993; Xie et al. 1994).

Table 3. Experimental data and rigid-body results for myosin

Property, molecule	Exptal	Rigid $L=$ 144 nm	Rigid $L=$ 150 nm	Rigid $L=$ 156 nm	Semi-flex Q
R_g, nm, rod	38	41	43	45	0.70
$[\eta]$, cm^3/g, rod	265	290	355	370	0.42
τ_1, rod		33	37	41	
R_g, nm, myosin	46	47		52	
$[\eta]$, cm^3/g, myosin	245	245		294	
τ_1, myosin		53		59	

Table 4. Individual relaxation times (μs) for myosin subunits, with different choices for the lengths (Å) rodlike parts. Results from Wegener (1992b)

Rod lengths			Myosin rod		Whole myosin		
L (rod)	L (S2)	L (LMM)	τ_{HW} (S2)	τ_{HW} (LMM)	τ_{HW} (S2)	τ_{HW} (LMM)	τ_{HW} (S1)
1440	430	1010	2.8	20.4	5.2	21.4	0.25
1440	720	720	9.5	9.5	15.1	9.9	0.26
1560	430	1130	2.9	27.0	5.3	28.4	0.25
1560	780	780	11.7	11.7	18.4	12.2	0.26
1440 (rigid)			37.6		51.6		0.27
1560 (rigid)			46.7		63.4		0.27

In conclusion, the question about myosin flexibility (particularly in the rod) is not solved as yet. From the theoretical side, the situation seems now clear, since the validity of the rigid-body and Harvey-Wegener treatments have been established, and Brownian dynamics simulation can provide further insight. It is hoped that this will stimulate new, carefully analyzed experiments.

Acknowledgements. During the writing of this review, the author was supported by grants PB90-0303 from Direction General de Universidad e Investigacion. M.E.C. and PIB 93/17 from Comunidad Autonoma de la Region de Murcia. Previous grants from these agencies are also acknowledged. Thanks are given to Prof. S. C. Harvey, Dr. P. Mellado, Dr. F. G. Diaz and Dr. A. Iniesta for their collaboration in some of the works reviewed here.

References

Abragam A (1978) The principles of Nuclear Magnetism. Chapt. VIII. Clarendon Press, Oxford

Allison SA (1986) Brownian Dynamics simulation of wormlike chains. Fluorescence depolarization and depolarized light scattering. Macromolecules 19:118–124

Allison SA, McCammon JA (1984a) Transport properties of rigid and flexible macromolecules by Brownian Dynamics simulation. Biopolymers 23:167–184

Allison SA, McCammon JA (1984b) Multistep Brownian dynamics: Application to short wormlike chains. Biopolymers 23:363–375

Allison SA, Soarlie SS, Pecora R (1990) Brownian Dynamics simulation of wormlike chains. Dynamic light scattering from a 2311 base pairs fragmente. Macromolecules 23:1110–1114

Allison SA, Nambi P (1992) Electric dichroism and electric birefringence decay of short DNA restriction fragments. A Brownian dynamics simulation. Macromolecules 25:759–769

Bayley P, Dale R (Eds) (1985) Spectroscopy and the Dynamics of Molecular Biological Systems. Academic Press, London

Berne B, Pecora R (1976) Dynamic Light Scattering. John Wiley, New York

Barbato G, Ikura M, Kay EL, Pastor RW, Bax A (1992) Backbone dynamics of calmodulin studied by NMR relaxation using inverse detected two-dimensional NMR spectroscopy: the central helix is flexible. Biochemistry 31:5269–5278

Bernengo JC, Cardinaud R (1982) State of myosin in solution. Electric birefringence and dynamical light scattering studies. J Mol Biol 159:501–517

Bloomfield VA, Dalton WO, Van Holde KE (1967) Frictional coefficients of multisubunit structures. I. Theory. Biopolymers 5:135–148

Bloomfield VA (1985a) Hydrodynamic properties of complex macromolecules. In: Bayley PM, Dale RE (eds) Spectroscopy and the dynamics of molecular biological systems. Academic Press, New York, pp 1–20

Bloomfield VA (1985b) Biological Applications. In: Pecora R (ed) Dynamic Light Scatterng. Application of photon correlation spectroscopy. Plenum Press, New York, pp 363–417

Bloomfield VA, Crothers DM, Tinoco I (1974) Physical chemistry of nucleic acids. Harper and Row, New York

Berne B, Pecora R (1976) Dynamic Light Scattering. John Wiley, New York

Burton DF (1987) Structure and function of antibodies, in: Molecular Genetics of Immunoglobulin, Calabi F, Neuberger MS (eds), Elsevier, Amsterdam, pp 1–50

Cardinaud R, Bernengo JC (1985) Electric birefringence study of rabbit skeletal myosin subfragments HMM, LMM and rod in solution. Biophys J 48:751–763

Cantor CR, Schimmel PR (1980) Biophysical chemistry, Parts II and III. Freeman, San Francisco

Ermak DL, McCammon JA (1978) Brownian dynamics with hydrodynamic interactions. J Chem Phys 69:1352–1357

Curry JF, Krause S (1991) On the flexibility of myosin in solution. Biopolymers 31:1677–1687

Dangl JL, Wensel TG, Morrison SL, Stryer L, Herzenberg LA (1988) Segmental flexibility and complement fixation of genetically engineered chimeric human, rabbit and mouse antibodies. EMBO J 7:1989–1994

Diaz FG, Iniesta A, Garcia de la Torre J (1987) Brownian dynamics simulation of rotational correlation functions of simple rigid models. J Chem Phys 87:6021–6027

Diaz FG, Garcia de la Torre J (1988) Simulation of the Brownian dynamics of a simple segmentally flexible model: The elastic trumbbell. J Chem Phys 88:7698–7705

Diaz FG, Iniesta A, Garcia de la Torre J (1990) Hydrodynamic study of flexibility in immunoglobulin IgG1 using Brownian dynamics simulation of a simple model. Biopolymers 29:547–554

Diaz FG, Garcia de la Torre J, Freire JJ (1990) Viscoelastic properties of simple flexible and semirigid models from Brownian dynamics simulation. Macromolecules 23:3144–3149

Diaz FG, Lopez Cascales JJ, Garcia de la Torre J (1993) Bead-model calculation of scattering diagrams. Brownian dynamics simulation study of flexibility in immunoglobulin IgG1. J Biochem Biophys Methods (in pess)

Diaz FG, Garcia de la Torre J (1994) Viscoelastic properties of semiflexible macromolecules: Brownian dynamics simulation of a trumbbell model. Macromolecules (in press)

Eads TM, Thomas DD, Austin RH (1984) Microsecond rotational motions of eosin-labeled myosin by time-resolved anisotropy of absorption and phosphorescence. J Mol Biol 179:55–81

Frederick E, Houssier C (1973) Electric Dichroism and Electric Birefringence. Clarendon Press, Oxford

Garcia de la Torre J (1981) Rotational diffusion coefficients. In: Krause S (ed) Molecular electro-optics. Plenum Press, New York, pp 75–103

Garcia de la Torre J (1989) Hydrodynamic properties of macromolecules assemblies. In: Harding SE, Rowe AJ (eds) Dynamic properties macromolecular assemblies. The Royal Society of Chemistry, pp 1–41

Garcia de la Torre J, Bloomfield VA (1977) Hydrodynamic properties of macromolecular complexes. I. Translation. Biopolymers 16:1747–1763

Garcia de la Torre J, Bloomfield VA (1978) Hydrodynamic properties of macromolecular complexes. IV. Intrinsic viscosity theory with applications to once broken rods and multisubunit proteins. Biopolymers 17:1605–1627

Garcia de la Torre J, Bloomfield VA (1980) The conformation of myosin in dilute solution as estimated from hydrodynamic properties. Biochemistry 19:5118–5123

Garcia de la Torre J, Bloomfield VA (1981) Hydrodynamic properties of complex, rigid, biological macromolecules. Theory and applications. Quart J Biophys 14:81–139

Garcia de la Torre J, Mellado P, Rodes V (1985) Diffusion coefficients of segmentally flexible macromolecules with two spherical subunits. Biopolymers 24:2145–2164

Garcia Molina JJ, Garcia de la Torre J (1984) Conformational properties of wormlike and hinged rods. A comparative study. In J Biol Macromol 6:170–174

Gregory L, Davis, KG, Sheth B, Boyd J, Jefferis R, Naves C, Burton D (1987) The solution conformations of the subclases of human IgG deduced from sedimentation and small angle X-ray scattering studies. Molecular immunology. Molecular Immunol. 24: 821–829

Hagerman P, Zimm BH (1981) Monte Carlo approach to the analysis of the rotational diffusion of wormlike chains. Biopolymers 20:1481–1502

Harding SE, Satelle DB, Bloomfield VA (eds) (1992) Laser Light Scattering in Biochemistry. The Royal Society of Chemistry, Cambridge

Harvey SC (1978) Diffusion of hinged particles: An exception to the Einstein relation. J Chem Phys 69:3426–3427

Harvey SC (1979) Transport properties of particles with segmental flexibility. I. Hydrodynamic resistance and diffusion of a freely hinged particle. Biopolymers 18:1081–1104

Harvey SC, Cheung H (1980) Transport properties of particles with segmental flexibility. II. Decay fluorescence polarization anisotropy from hinged macromolecules. Biopolymers 18:1081–1104

Harvey SC, Cheung H (1982) Myosin Flexibility. In: Cell and Muscle Motility, Vol. 2. Dowben RM, Shay JW (eds), Plenum Press, New York, pp 279–302

Harvey SC, Mellado P, Garcia de la Torre J (1983) Hydrodynamic resistance and diffusion coefficients of segmentally flexible macromolecules with two subunits. J Chem Phys 78:2081–2090

Hassager O (1974) Kinetic theory and rheology of bead-rod models for macromolecular solutions. I. Equilibrium and steady flow properties. J Chem Phys 60:2111–2124

Highsmith S, Wang CC, Zero K, Pecora R, Jardetzki O (1982) Bending motions and internal motions in myosin rod. Biochemistry 21:1192–1200

Hvidt S, Henry F, Greaser ML, Ferry JD (1982) Flexibility of myosin rod determined from dilute solution viscoelastic measurements. Biochemistry 21:4064–4073

Hvidt S, Chang T, Yu H (1984) Rigidity of myosin and myosin rod by electric birefringence. Biopolymers 23:1283–1294

Huxley HE (1971) The structural basis of muscular contraction. Proc Roy Soc London Ser B 160:442–472

Iniesta A, Garcia de la Torre J (1987) Rotational diffusion coefficients of a small spherical subunit flexibly thethered to a larger sphere. Eur Biophys J 14:493–498

Iniesta A, Garcia de la Torre J (1989) Electric birefringence of segmentally flexible macromolecules with two subunits. J Chem Phys 90:5190–5197

Iniesta A, Diaz FG, Garcia de la Torre J (1988) Transport properties of rigid bend-rod macromolecules and semiflexible broken rods in the rigid body approximation. Biophys J 54:269–275

Iniesta A, Garcia de la Torre J (1990) A second-order algorithm for the simulation of the brownian dynamics of macromolecules models. J Chem Phys 92:2015–2019

Iniesta A, Lopez Martinez MC, Garcia de la Torre J (1991) Rotational brownian dynamics of semiflexible broken rods. J Fluorescence 1:129–134

Jennings BR (1985) Electric field orientation and macromolecular relaxation. In: Bayley PM, Dale RE (eds) Spectroscopy and the dynamics of molecular biological systems. Academic Press, New York, pp 21–34

Jorquera H, Qin L, Dahler JS (1990) Steady, elongational flow of dilute solutions of once-bent, once-broken, and deformable rod polymers. J Chem Phys 93:2116–2124

Lewis RG, Allison SA, Eden D, Pecora R (1988) Brownian dynamics simulations of a three-subnit and ten-subunit wormlike chain: Comparison with trumbbell theory and with experimental results from DNA. J Chem Phys 89:2490–2503

Lopez-Lacomba JL, Guzmn M, Cortijo M, Mateo P, Aguirre R, Harvey SC (1989) Differential scanning calorimetric study of the thermal unfolding of myosin rod, light meromyosin, and subfragment 2. Biopolymers 28:2115–2142

Kinoshita K, Ishiwta S, Yoshimura H, Asai H, Ikegami A (1984) Submicrosecond and microsecond rotational motions of myosin head in solution and in myosin synthetic filaments as revealed by time-resolved optical anisotropy decay. Biochemistry 23:5963–5975.

Mellado P, Garcia de la Torre J (1982) Steady state and transient electric birefringence of solutions of bent-rod macromolecules. Biopolymers 21:1857–1871

Mellado P, Iniesta A, Diaz FG, Garcia de la Torre J (1988) Diffusion coefficients of segmentally flexible macromolecules with two subunits. Study of broken rods. Biopolymers 27:1771–1786

Moro K, Fujiwara M (1986) Initial relaxation times in dynamic light scattering from one-broken rod molecules in solution. J Polym Sci Phys Ed 24:2403–2421

Matsumoto T, Nishioka , Teramato A, Fujita H (1975) Dielectric dispersion of polypeptide solutions. I. Once-broken rod polypeptide based on γ-benzyl L-glutamate. Macromolecules 7: 824–831

Muroaga Y, Tagawa H, Hiragi Y, Ueki T, Kataoka M, Izuni Y, Aneniya Y (1988) Conformational analysis of broken rodlike chains. 2. Conformational analysis of poly(D-glutamic acid) in aqueous solution by small-angle x-ray scattering. Macromolecules 21:2760–2765

Nagasaka K, Yamakawa H (1985) Dynamics of weakly bending rods. A trumbbell model. J Chem Phys 83:6480–6488

Oi VT, Vuong TM, Hardy R, Reidler J, Dangl J, Herzenberg LA, Stryer L (1984) Correlation between segmental flexibility and effector function of antibodies. Nature 307:136–140

Rau D (1993) Calculation of birefringence signal kinetics for coupled motion with myosin II filaments. J Biol Chem 268:4622–4624

Rau D, Ganguly C, Korn ED (1993) A structural difference between filaments of phosphorilated and dephosphorilated Acanthamoeba myosin II revealed by electric birefringence. J Biol Chem 268: 4612–4621

Rayement I, Rypniewski WR, Schmidt-Bäse K, Smith R, Tomchick DR, Benning MM, Winkelmann DA, Wesenberger G, Holden HM (1993) Three-dimensional structure of myosin subfragment-1: A molecular motor. Science 261:50–58

Richards EG (1980) An introduction to the physical properties of large molecules in solution. Cambridge University Press, Cambridge

Roitman DB (1984) An elastic hinge model for the dynamics of stiff chains. III. Viscoelastic properties and Kerr-effect behavior of bent molecule. J Chem Phys 81:6356–6360

Roitman DB, Zimm BH (1984a) An elastic hinge model for the dynamics of stiff chains. I. Viscoelastic properties. J Chem Phys 81:6356–6360

Roitman DB, Zimm BH (1984b) An elastic hinge model for the dynamics of stiff chains. II. Transient electro-optical properties. J Chem Phys 81:6348–6355

Solvez A, Iniesta A, Garcia de la Torre J (1988) Radius of gyration of multisubunits macromolecules. Theory and application to myosin heads, myosin rods and whole myosin. Int J Biol Macromolecules 9:39–43

Tirado MM, Garcia de la Torre J (1979) Translational friction coefficients of rigid, symmetric top macromolecules. Application to circular cylinders. J Chem Phys 71:2581–2587

Tirado MM, Garcia de la Torre J (1980) Rotational dynamics of rigid, symmetric top macromolecules. Application to circular cylinders. J Chem Phys 73:1986–1993

Tirado MM, Lopez Martinez MC, Garcia de la Torre J (1984) Comparison of theories for the translational and rotational diffusion coefficients of rodlike macromolecules. Application to short rodlike cylinders. J Chem Phys 81:2047–2052

Ulyanova NY, Baranovskaya IA, Liubina SY, Berzukova MA (1991) Investigation of macromolecules exhibiting the structure of a once-broken rod by molecular optics. 1. Synthesis and investigation of poly(benzyl-L-glutamate) with short joints. Macromolecules 24:3319–3324

Wegener WA (1980) Hydrodynamic resistance and diffusion coefficients of a freely hinged rod. Biopolymers 19:1899–1908

Wegener WA (1982a) Bead models of segmentally flexible macromolecules. J Chem Phys 76:6425–6430

Wegener WA (1982b) A swivel-joint formalism for segmentally flexible macromolecules and its application to the rotational behavior of myosin. Biopolymers 21:1049–1080

Wegener WA (1985) Center of diffusion of flexible macromolecules. Macromolecules 18:2522–2530

Wegener WA, Dowben RM, Koester VJ (1979) Time-dependent birefringence, linear dichroism and optical rotation resulting from rigid- ody rotational diffusion. J Chem Phys 70:622–632

Wegener WA, Dowben RM Koester VJ (1980) Diffusion coefficients for segmentally flexible macromolecules: general formalism and application to rotational behavior of a body with two segments. J Chem Phys 73:4086–4097

Xie X, Harrison DH, Schlichting I, Sweet RM, Kalabokis VN, Szent-Györgyi AG, Cohen C (1994) Structure of the regulatory domain of scallop myosin at 2.8 A resolution. Nature 368:306–312

Yamakawa H (1971) Modern theory of polymer solutions. Harper and Row, New York

Yguerabide J, Epstein HF, Stryer L (1970) Segmental flexibility in an antibody molecule. J Mol Biol 51:573–588

Yu H, Stockmayer WH (1967) Intrinsic viscosity of a once-broken rod. J Chem Phys 47:1369–1373

Zero K, Pecora R (1982) Restricted flexing of once-broken rods. Macromolecules 15:1023–1027